Supporting Information

Mechanical and Viscoelastic Properties of Polymer-Grafted Nanorod Composites from Molecular Dynamics Simulation

Jianxiang Shen[1*], Xue Li[2], Liqun Zhang[3], Xiangsong Lin[1], Haidong Li[1],Xiaojun Shen[1], and Venkat Ganesan[4*], and Jun Liu[3*]

[1]Department of Polymer Science and Engineering, Jiaxing University, Jiaxing314001, P. R. China

[2]Department of Chemical and Textile Engineering, Jiaxing University Nanhu College, Jiaxing314001, P. R. China

[3]Key Laboratory of Beijing City on Preparation and Processing of Novel Polymer Materials, Beijing University of Chemical Technology, Beijing 100029, P. R. China

[4]Department of Chemical Engineering, The University of Texas, Austin, USA

Corresponding authors

*Email: shenjx@mail.zjxu.edu.cn (J. Shen); liujun@mail.buct.edu.cn (J. Liu); venkat@che.utexas.edu (V. Ganesan)

Number of Pages: 15

Number of Figures: 16

*Corresponding authors:
shenjx@mail.zjxu.edu.cn (J. Shen); liujun@mail.buct.edu.cn (J. Liu); venkat@che.utexas.edu (V. Ganesan)

CONTENTS

N_g=10, and the grafted chain length is L_g=6.

Figure S12. Average bridging contacts of matrix chains with two grafted layers or NRs with regard to (a) grafting density and (b) grafted chain length.

Part II. Computation of side-by-side alignment and site-to-site contact between NRs

Figure S13. (a) Side-by-side alignment; (b) Snapshot of our PNC system filled with bare-NRs. For clarity, matrix chains are not shown.

Figure S14. Three types of misalignment: (a) Radial misalignment; (b) Axial misalignment; and (c) Angular misalignment.

Figure S15. (a) Unit direction vector $\mathbf{D}_0$ in three dimensional Cartesian coordinate system; (b) The angle between two vectors.

Part III. Curving-fitting of the stress-strain relation calculated in the tensile test

Figure S16. The stress-strain curve of the N_g=4 system calculated in the tensile test and its nonlinear curve-fittings.

Part I. Characterization of NR dispersion state and the NRs/polymer interface

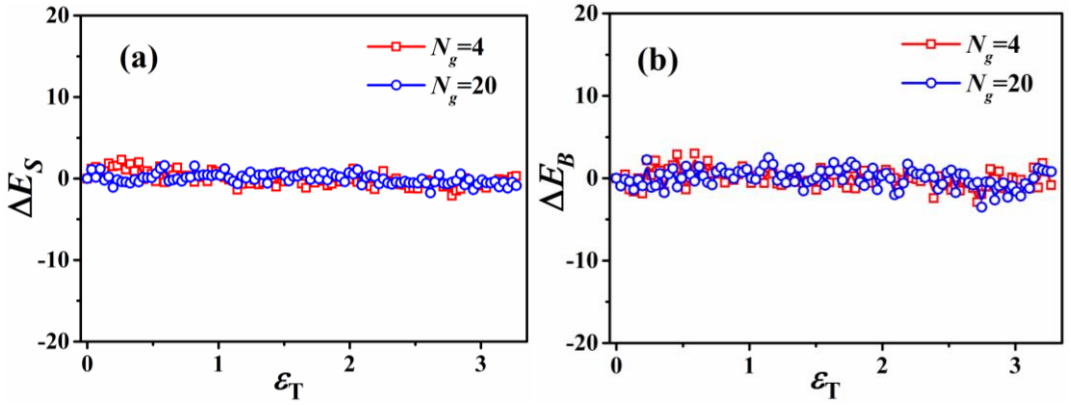

Figure S1. The changes of (a) stretching energy and (b) bending energy of the nanorods (NRs) during the tensile process. The grafting density is equal to $N_g = 4$ and $N_g = 12$, respectively, and the grafted chain length is $L_g = 6$.

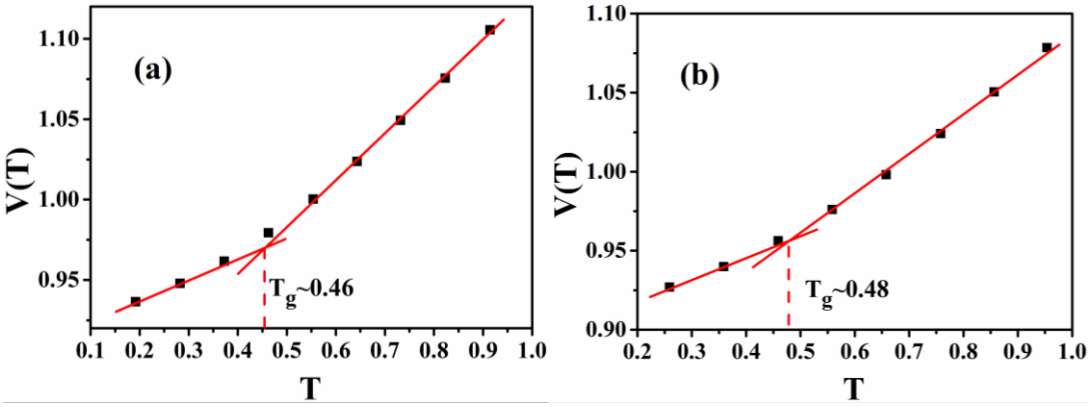

Figure S2. Plots of the specific volume V(T) with respect to temperature for (a) pure polymer and (b) 5V% NR-filled polymer. The cooling rate is set as $0.01\tau^{-1}$.

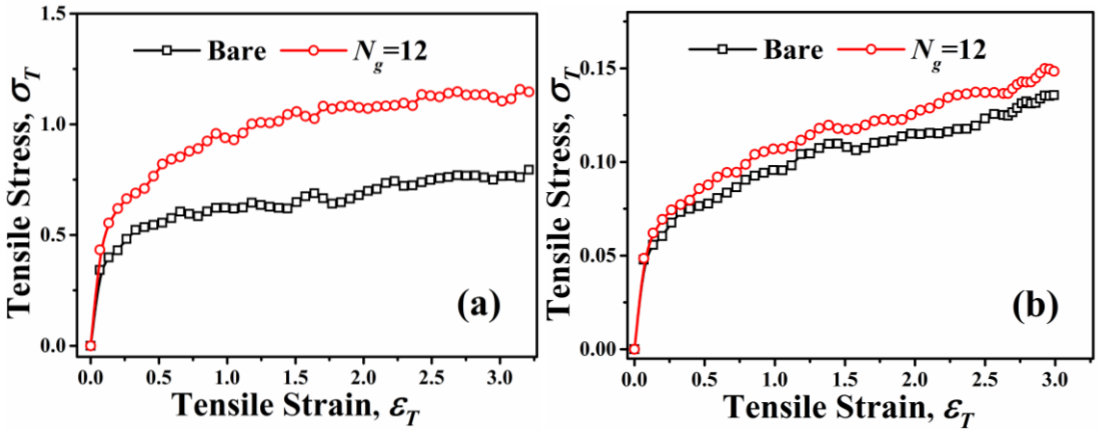

Figure S3. Comparison of stress-strain curves for different systems at tensile rate of (a) 0.0327/τ and (b) 0.00327/τ

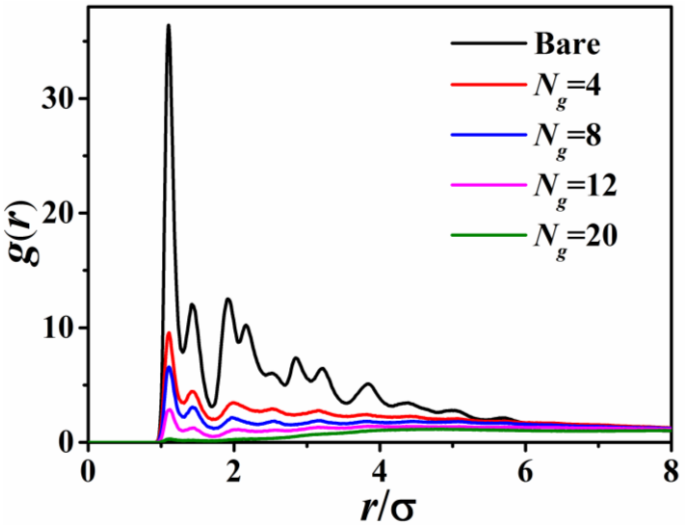

Figure S4. Inter-rod radial distribution functions *g(r)* corresponding to different grafting densities (N_g). The grafted chain length is $L_g = 6$.

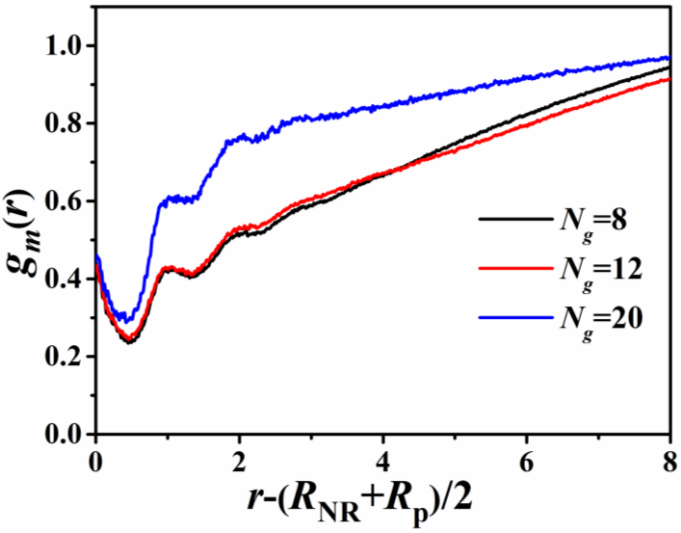

Figure S5. Influence of grafting density on the monomer density profiles of matrix chains as a function of separation from the NR surface.

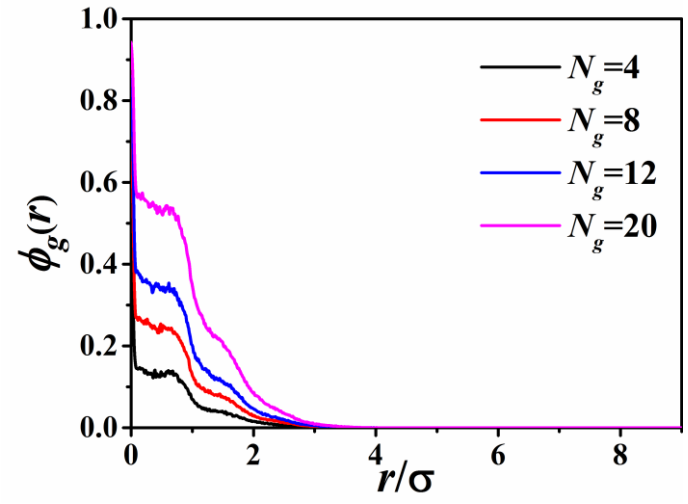

Figure S6. Monomer density profiles as a function of position from the NR diametrical axis of grafted chains that are grafted to the reference NR. The curves are shifted by the NR radius.

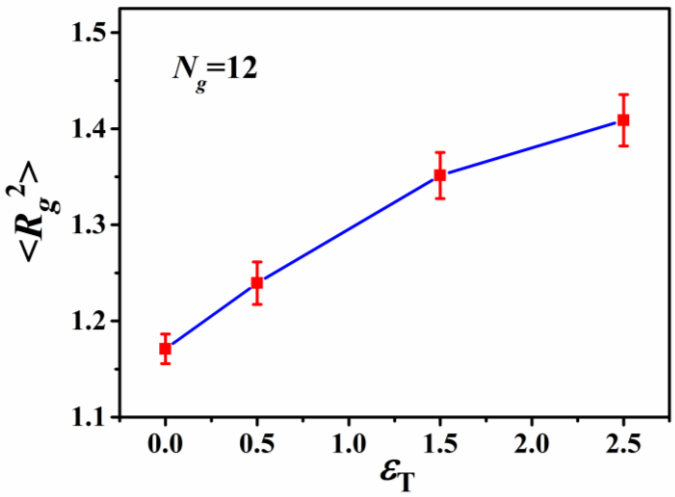

Figure S7. Mean-square radius of gyration of grafted chains plotted vs. tensile strain. The grafting density is $N_g = 12$ and the grafted chain length is $L_g = 6$.

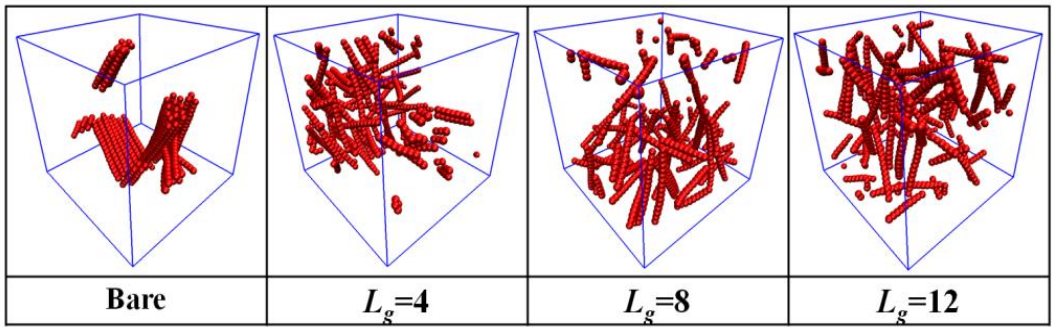

Figure S8. Snapshots of NR-filled polymer systems with different grafted chain lengths (L_g).

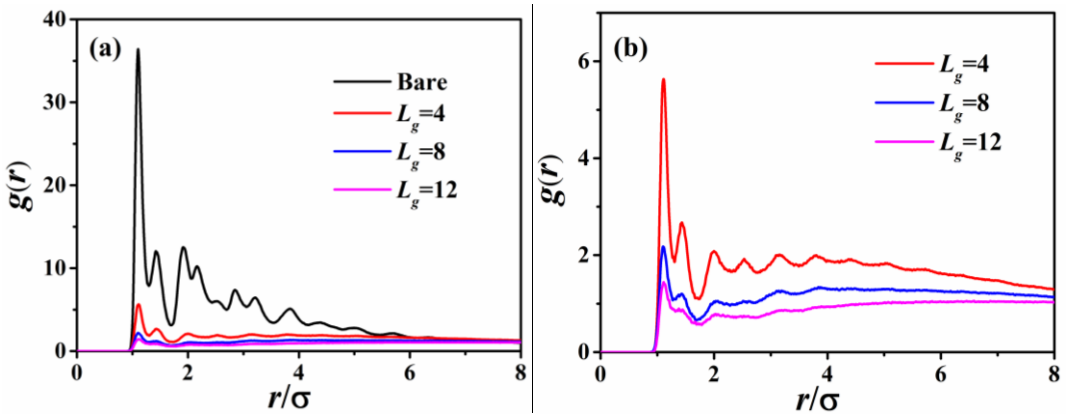

Figure S9. Inter-rod radial distribution functions *g(r)* corresponding to different grafted chain lengths (L_g). For better comparison, the bare system is not shown in Figure S9b. The grafting density is $N_g = 10$.

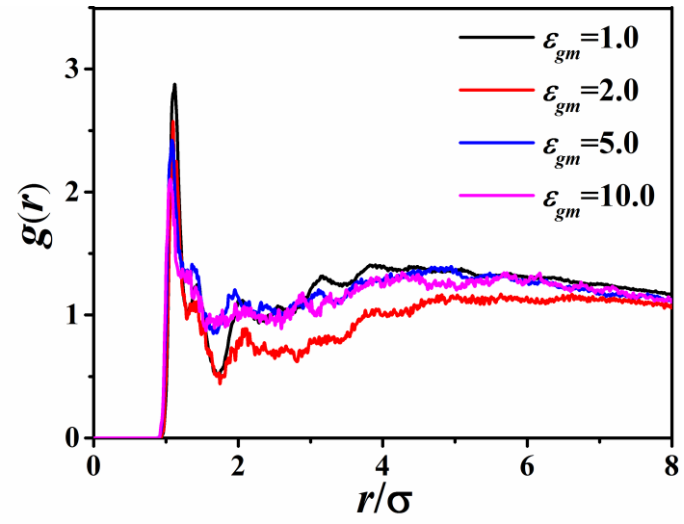

Figure S10. Inter-rod radial distribution functions *g(r)* corresponding to different graft-matrix interactions (ε_{gm}). The grafting density is $N_g = 12$, and the grafted chain length is $L_g = 6$.

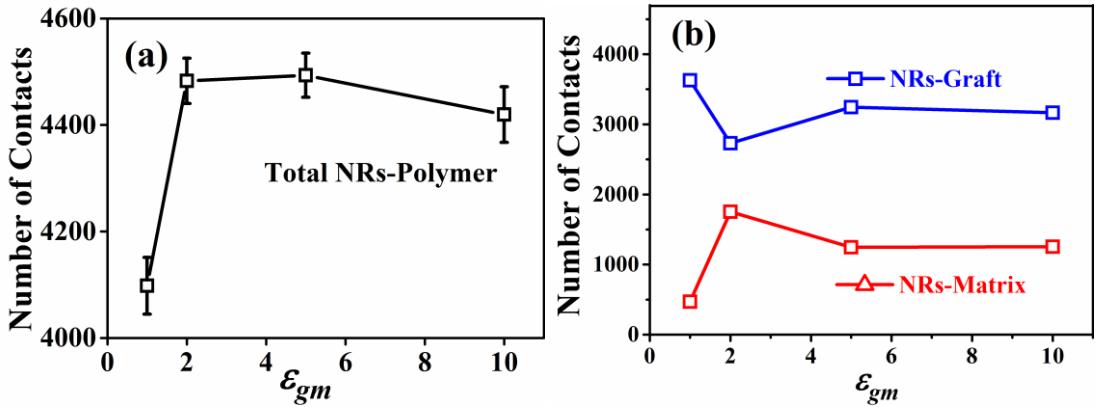

Figure S11. (a) Total number of direct contacts of NRs with polymer segments as a function of the graft-matrix interaction (ε_{gm}); (b) Direct contacts of NRs with grafted chain segments and matrix chain segments. The grafting density is $N_g = 12$, and the grafted chain length is $L_g = 6$.

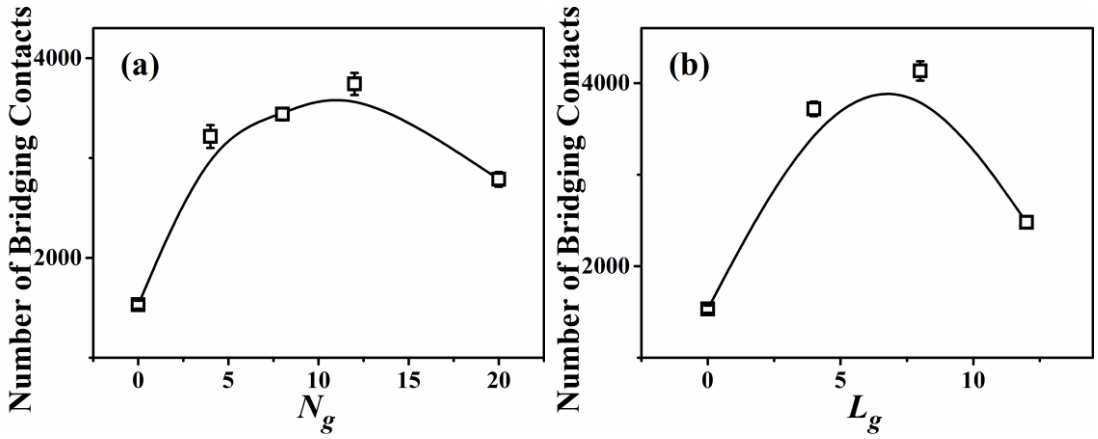

Figure S12. Average bridging contacts of matrix chains with two grafted layers or NRs with regard to (a) grafting density and (b) grafted chain length.

Part II. Computation of side-by-side alignment and site-to-site contact between NRs

As the rigid NRs in our simulations can be regarded as incompressible neo-Hookean solids (see Figure S1), we can borrow the definition of shaft alignment from mechanical engineering. As illustrated by Figure S13, for two NRs to be called "side-by-side aligned", their shaft centerlines need to be parallel, and meanwhile the distance between their center of mass needs to be equal to the diameter of NR. Besides, there are three types of misalignment, i.e., radial misalignment, axial misalignment, and angular misalignment, as sketched in Figure S14.

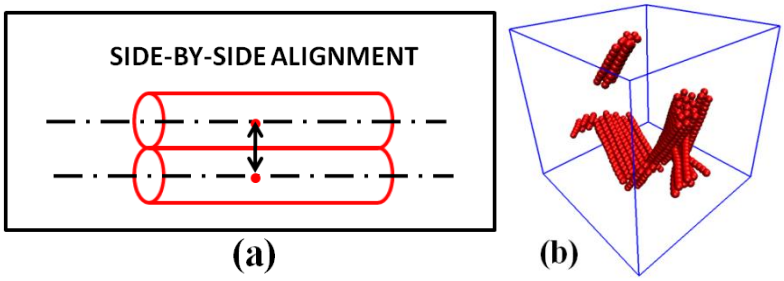

Figure S13. (a) Side-by-side alignment; (b) Snapshot of our PNC system filled with bare-NRs. For clarity, matrix chains are not shown.

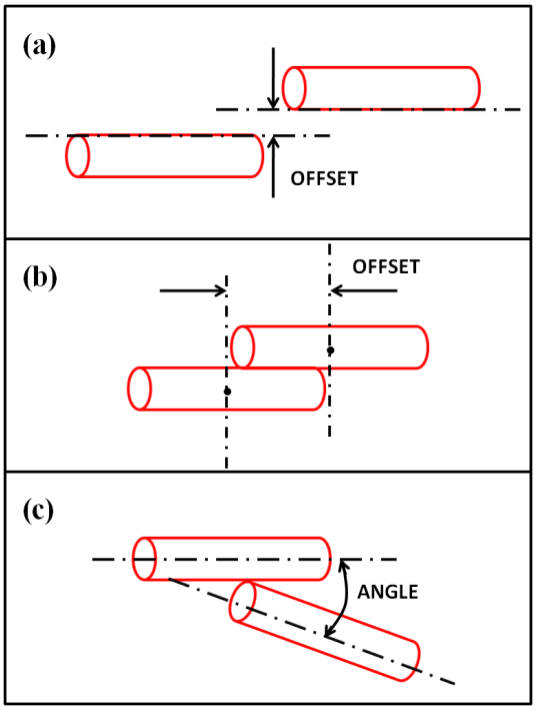

Figure S14. Three types of misalignment: (a) Radial misalignment; (b) Axial misalignment; and (c) Angular misalignment

However, within our NR model the perfect arrangement of NRs aligning side-by-side is not likely to exist as a persistent state in our simulations. As the NR in our simulation is constructed through the bead-spring model, despite the tight constraint imposing the NR beads by the stiff harmonic potential and bending potential, the NR beads can still move slightly around their thermodynamic equilibrium position, even if they are in the side-by-side alignment state. In that case, the perfect side-by-side alignment of NRs would be instantaneous, and probably two NR could be mostly aligned parallel to each other but with a slight angle between them, which can be also confirmed by the snapshot in Figure S13(b). Taking into account the possibility of imperfect side-by-side alignment, we expand the definition of side-by-side alignment. To this end, a weaker criterion of "side-by-side alignment" is used to include the slight misalignment caused by the thermal motion of NR beads, as follows:

1. Angular misalignment: At the beginning, a simple linear-fitting procedure is applied to determine the shaft centerline of each rigid NR with the unit direction vector $\mathbf{D}_0(x_0, y_0, z_0)$. As illustrated in Figure S15(a), the 3 components of vector $\mathbf{D}_0(x_0, y_0, z_0)$ are equal to the cosine of their corresponding direction angle ($x_0 = \cos\alpha$, $y_0 = \cos\beta$, $z_0 = \cos\gamma$, and $x_0^2 + y_0^2 + z_0^2 = 1$). Then, we need a criterion to judge whether any two shaft centerlines are in the "acceptable" parallel orientation. Here for our measurement, two NRs are considered to be acceptably parallel only when the angle between the two direction vectors of their shaft centerlines is less than the small angle of $\theta \le 8^\circ$, as shown in Figure S15(b). Using the vector inner product, the acceptable side-by-side alignment of NRs is expressed as follows:

$$\cos\theta = \frac{\mathbf{D}_1 \bullet \mathbf{D}_2}{\|\mathbf{D}_1\|\|\mathbf{D}_2\|} = \frac{x_1x_2 + y_1y_2 + z_1z_2}{\sqrt{x_1^2 + y_1^2 + z_1^2}\sqrt{x_2^2 + y_2^2 + z_2^2}} \ge 0.99 \quad or \quad \le -0.99 \qquad (2.1)$$

where $\cos\theta \ge 0.99$ holds for two vectors in the same direction, and $\cos\theta \le -0.99$ for the vectors in the opposite direction. Our setting of this angle (8°) is driven by two considerations: first, the angle should be appropriately large so that the slight

misalignment caused by the thermal motion of NR beads can be fully covered; second, when the first condition is satisfied, the angle value should be sufficiently small.

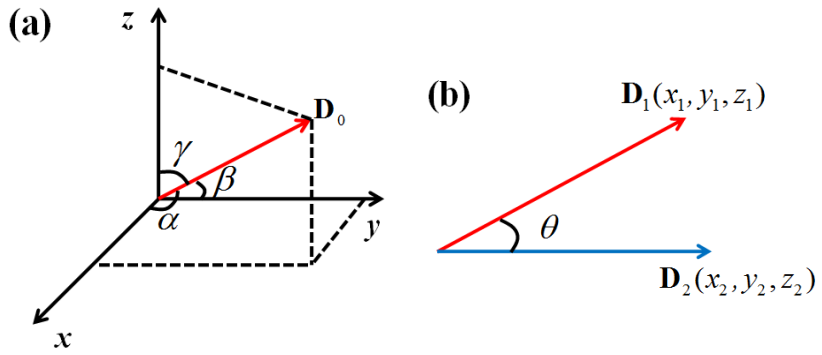

Figure S15. (a) Unit direction vector $\mathbf{D}_0$ in three dimensional Cartesian coordinate system; (b) The angle between two vectors

2. Axial misalignment: For two NRs in the angular alignment, their unit direction vectors can be unified as $\mathbf{D}_0(x_0, y_0, z_0)$, and the position vector from the center of one NR to the other can be expressed as $\mathbf{D}_c(x_1, y_1, z_1)$. Consequently, using the vector operation, we can obtain the axial offset, as follows:

$$D_A = \left| \frac{\mathbf{D}_c \bullet \mathbf{D}_0}{\|\mathbf{D}_0\|} \right| = \frac{|x_1 x_0 + y_1 y_0 + z_1 z_0|}{\sqrt{x_0^{\,2} + y_0^{\,2} + z_0^{\,2}}} = |x_1 x_0 + y_1 y_0 + z_1 z_0| \qquad (2.2)$$

In our standard of acceptable axial misalignment, the axial offset should be no more than the distance between two adjacent NR beads, i.e., $D_A \le 0.66\sigma$.

3. Radial misalignment: Given the distance between two centers of NRs and the axial offset, we then obtain the radial offset D_R by the laws of geometry. The radial offset should be no more than the radius of NR beads, i.e., $D_R \le 0.5\sigma$.

Although the choices of maximum permissible angle, axial offset and radial offset are arbitrary, the appropriateness of our choice is reflected by the slight fluctuation in the side-by-side alignment in equilibrium state and also the changes of side-by-side alignment being well-correlated to the mechanical behavior. Besides, a simple validation of our computation method is to count the NRs in side-by-side alignment one by one in several representative snapshots.

Now that the definition of "side-by-side alignment" has been clarified, the characterization of "site-to-site contact" is easier to understand. The site-to-site contacts between two NRs refer to the direct contacts between those which are *not* side-by-side aligned to each other, such as the end-to-end and end-to-side contacts. Those NRs which have no contact with all other NRs are classified as isolated NRs. By the way, the NRs which are side-by-side aligned to at least one other NR are categorized as NRs in side-by-side alignment, while the NRs contacting with other NRs only by site-to-site are categorized as NRs via site-to-site contact. According to our simulation results, when the simulation system reaches equilibrium, the site-to-site aggregates and side-by-side aggregates hardly transform into each other. However, with the increase of grafting density or grafted chain length, the side-by-side aggregates are most likely to transform into site-to-site aggregates, into isolated NRs. The transformation between them will also occur during the deformation process.

As the NR is likely to be side-by-side aligned to one NR but site-to-site contacts with the other, we then use the ensemble averaged coordination number, C_n, which is defined as the average number of neighboring NR beads (connected by either site-to-site or side-by-side). Two NR beads belonging to different NRs are considered to contact with each other (or "neighboring") if their center-to-center distance is smaller than 1.25σ. That is to say, the cutoff distance for the calculation of the averaged coordination number is 1.25σ.

Part III. Curving-fitting of the stress-strain relation calculated in the tensile test

In order to obtain a smooth elastic modulus-strain curve, we need to first fit the stress-strain curve with an appropriate function and subsequently calculate the derivative. Considerable effort has been devoted to the stress-strain relation of polymers, such as the famous semi-empirical Mooney-Rivlin equation

$$\sigma = (C_1 + \frac{C_2}{\lambda})(\lambda - 1/\lambda^2)$$

where the parameter C_1 denotes the contribution of chemical cross-links, and the parameter C_2 denotes the entanglement contribution.

We list some other well-known nonlinear stress-strain relations below:

$$\sigma = (C_1 + \frac{1.84C_2}{\lambda + 0.84/\sqrt{\lambda}})(\lambda - 1/\lambda^2) \quad \text{(ref. 1)} \qquad (3.1)$$

$$\sigma = (C_1 + \frac{C_2}{\lambda - 1/\sqrt{\lambda} + 1})(\lambda - 1/\lambda^2) \quad \text{(ref. 2)} \qquad (3.2)$$

$$\sigma = (C_1 + \frac{C_2}{0.72\lambda + 0.61/\sqrt{\lambda} - 0.35})(\lambda - 1/\lambda^2) \quad \text{(ref. 3)} \qquad (3.3)$$

However, these stress-strain relations with two adjustable parameters only apply to unfilled cross-linked polymer networks. As we discussed in detail in our previous paper[ref. 4], these equations are not suitable for our PNC systems, with the square of correlation coefficient (R^2) much lower than 1.0.

In an attempt to better fit the simulated stress-strain curves, we proposed a modified stress-strain equation with three additional parameters so as to take in the effects of fillers. The equation is expressed as

$$\sigma = (C_1 + \frac{C_2}{C_3 * \lambda + C_4/\sqrt{\lambda} + C_5})(\lambda - 1/\lambda^2) \quad \text{(ref. 4)} \qquad (3.4)$$

Although the parameters C_1 and C_2 are known to describe the cross-linking effect and the entanglement effect respectively, the physical meaning of the additional

three parameters (C_3, C_4 and C_5) are however not get clear. Thus, this modified stress-strain equation is based purely on mathematical considerations. Nevertheless, it fits the simulated stress-strain curves well with R^2=0.99, as shown in Figure S16.

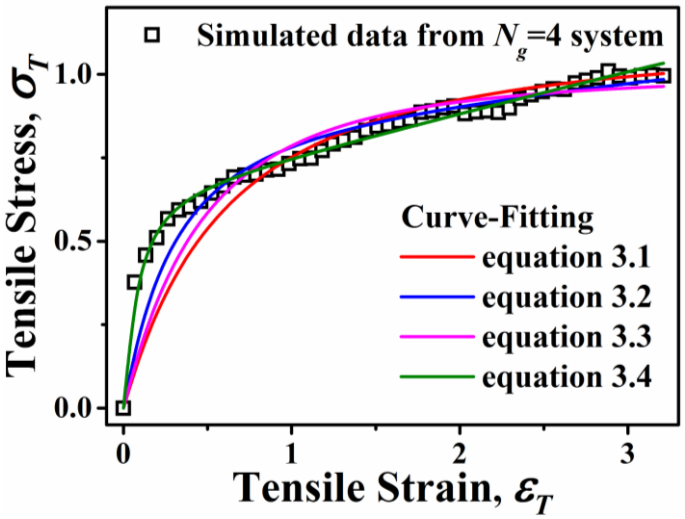

Figure S16. The stress-strain curve of the N_g=4 system calculated in the tensile test and its nonlinear curve-fittings.

REFERENCES

(1) Grest, G. S.; Pütz, M.; Everaers, R.; Kremer, K. Stress-strain relation of entangled polymer networks. *Journal of Non-Crystalline Solids* **2000,** *274*, 139-146.

(2) Rubinstein, M.; Panyukov, S. Elasticity of Polymer Networks. *Macromolecules* **2002,** *35*, 6670-6686.

(3) Rottach, D. R.; Curro, J. G.; Budzien, J.; Grest, G. S.; Svaneborg, C.; Everaers, R. Permanent Set of Cross-Linking Networks: Comparison of Theory with Molecular Dynamics Simulations. *Macromolecules* **2006,** *39*, 5521-5530.

(4) Shen, J.; Liu, J.; Gao, Y.; Li, X.; Zhang, L. Elucidating and tuning the strain-induced non-linear behavior of polymer nanocomposites: a detailed molecular dynamics simulation study. *Soft Matter* **2014,** *10*, 5099-5113.